

QUARK-NOVAE IN LOW-MASS X-RAY BINARIES WITH MASSIVE NEUTRON STARS: A UNIVERSAL MODEL FOR SHORT-HARD GAMMA-RAY BURSTS

RACHID OUYED¹, JAN STAFF², AND PRASHANTH JAIKUMAR^{3,4}

Department of Physics and Astronomy, University of Calgary, 2500 University Drive NW, Calgary, Alberta, T2N 1N4 Canada
 Department of Physics and Astronomy, Louisiana State University, 202 Nicholson Hall, Tower Dr., Baton Rouge, LA 70803-4001, USA
 Department of Physics and Astronomy, California State University Long Beach, 1250 Bellflower Blvd., Long Beach CA 90840 and
 Institute of Mathematical Sciences, CIT Campus, Taramani, Chennai 600113, India

Draft version January 18, 2011

ABSTRACT

We show that several features reminiscent of short-hard Gamma-ray Bursts (GRBs) arise naturally when Quark-Novae occur in low-mass X-ray binaries born with massive neutron stars ($\geq 1.6M_{\odot}$) and harboring a circumbinary disk. Near the end of the first accretion phase, conditions are just right for the explosive conversion of the neutron star to a quark star (Quark-Nova). In our model, the subsequent interaction of material from the neutron star's ejected crust with the circumbinary disk explains the duration, variability and near-universal nature of the prompt emission in short-hard GRBs. We also describe a statistical approach to ejecta break-up and collision to obtain the photon spectrum in our model, which turns out remarkably similar to the empirical Band function (Band et al. 1993). We apply the model to the fluence and spectrum of GRB 000727, GRB 000218, and GRB980706A obtaining excellent fits. Extended emission (spectrum and duration) is explained by shock-heating and ablation of the white dwarf by the highly energetic ejecta. Depending on the orbital separation when the Quark-Nova occurs, we isolate interesting regimes within our model when both prompt and extended emission can occur. We find that the spectrum can carry signatures typical of Type Ib/c SNe although these should appear less luminous than normal type Ib/c SNe. Late X-ray activity is due to accretion onto the quark star as well as its spin-down luminosity. Afterglow activity arise from the expanding shell of material from the shock-heated expanding circumbinary disk. We find a correlation between the duration and spectrum of short-hard GRBs as well as modest hard-to-soft time evolution of the peak energy.

Subject headings: Stars: evolution, stars: binary, stars: neutron, supernovae: general, gamma-ray burst: general

1. INTRODUCTION

Intensive sampling of gamma-ray burst (GRB) light curves by *Swift* has revealed that at least in some short GRBs (henceforth shGRBs), prompt emission is followed by softer, extended emission lasting tens to hundreds of seconds. For example, the lightcurve of GRB 050709 (Villasenor et al. 2005) has a short-hard pulse $T_{90} \sim 0.2$ s and a long-soft pulse $T_{90} \sim 130$ s; GRB 050724 (Barthelmy et al. 2005) has prominent emission lasting for ~ 3 s followed by a long, soft, less prominent emission peaking at ~ 100 s after the trigger, while XRT observations reveal strong flare-like activities within the first hundreds of seconds. In GRB 060614, the lightcurve has a short-hard episode followed by an extended soft emission component with strong spectral evolution. On average, the principal properties of the intense prompt component (< 2 s) of short bursts with and without extended emission (EE) are indistinguishable, suggesting that short bursts are “universal” (Norris & Gehrels 2008). While the origin of such extended emission (seen roughly in a quarter of *Swift* shGRBs) is debated, it can provide some clues to the identity of the elusive mechanism of shGRBs.

The association of some shGRBs with early type galaxies that have low star formation rates suggests that short bursts arise from a different progenitor mecha-

nism than long bursts and that neutron star-black hole (NS-BH) or double neutron star (NS-NS) mergers might be at play (Bloom&Prochaska 2006). But how does one obtain extended emission in this case? Extended accretion episodes in NS-BH mergers have been proposed (Barthelmy et al. 2005), while Rosswog (2006) suggest that some debris may be launched during the merger process, which would fall back later to power flares at late times. Alternatively, disk fragmentation (Perna et al. 2006) or magnetic field barrier near the accretor (Proga & Zhang 2006) may induce intermittent accretion that power the flares. Other types of mergers such as a white dwarf-neutron star (WD-NS) merger (King et al. 2007) have been advanced to interpret shGRBs. Dai et al. (2006) argue that the final product of a NS-NS merger may be a heavy, differentially-rotating NS, whose post-merger magnetic activity would give rise to flares following the merger events. The ‘off axis collapsar’ models (Lazzati et al. 2010) and the millisecond magnetar model (Metzger et al. 2008) offer explanations for why the extended emission from short GRBs may resemble the prompt emission from long GRBs. However, it is unclear how this model can explain the apparent different galactic environments in which short and long GRBs are found. In both types of bursts, the photon spectrum is well fitted by the Band function, hinting at a kind of universality in the underlying physical model.

Here, we will explore an alternative model based on a Quark-nova explosion occurring in a low mass X-ray binary (LMXB). Such an explosion can happen if the neutron star, in its spin-down evolution, reaches the quark deconfinement density and subsequently undergoes a phase transition to the more stable strange quark matter phase (Itoh 1970; Bodmer 1971; Witten 1984), resulting in a conversion front that propagates towards the surface in the detonative regime. This hypothesis is motivated by recent work on numerical simulations of the conversion of neutron matter to strange quark matter (Niebergal et al. 2010b). Previous works that have focused either exclusively on conversion through strange matter diffusion (eg. Olinto 1987; Horvath&Benvenuto 1988) or use pure hydrodynamics (eg. Drago et al. 2007; Cho et al. 1994) do not find detonation, only deflagration. However, in the most recent work on this matter (Niebergal et al. 2010b), we have analyzed the issue numerically including both reaction-diffusion *and* hydrodynamics consistently, albeit within a 1D approximation. We also included for the first time, the effects of neutrino cooling, finding numerical evidence for laminar speeds approaching $0.04c$ (much higher than previous works; c is the speed of light) and a possible wrinkling instability in higher dimensions. As argued recently by Horvath (2010), wrinkles cause turbulence in the conversion front that serve as a platform for detonation. If this is borne out by more sophisticated simulations, we will have found potentially a new engine for GRBs that is capable of explaining several features of the GRB light curve, as we show in this work. This exciting possibility, combined with the problems faced by more conventional scenarios described in the previous paragraph, should make our model worth exploring as a possible option.

We note that Niebergal et al. (2010b) is already an important step forward in resolving some of the issues with uncertainties in the dynamics of the Quark-Nova. The equation of state of quark matter, and hence the putative quark deconfinement density is also unconstrained, but recently Özel & Psaltis (2009) have argued that accurate measurement of mass and radius for a minimum of three neutron stars will provide strong constraints up to several times nuclear saturation density. While we must await future observations of neutron star parameters for the resolution of some of these issues on the underlying Quark-Nova dynamics to be more confident in our model assumptions, we nevertheless adopt a *working hypothesis* in this paper that the detonative regime is indeed the likely result of a quark-hadron phase transition inside a neutron star. From this point on, we will follow standard arguments to demonstrate that a Quark-Nova occurring in an LMXB following the end of the first accretion phase leads to features (prompt emission, extended emission and flaring) reminiscent of those discussed above in the context of short GRBs as observed by *Swift*. The same engine at play inside a collapsar can naturally explain the many similarities between short and long duration GRBs, thus exhibiting universality between the two classes. In the end, we obtain many observed features of short GRBs beginning with our single hypothesis of the detonative transition, implying that shGRBs could well provide the astrophysical evidence for the Quark-nova, and that this mechanism deserves detailed study.

This paper is organized as follows: In §2 we describe the LMXB parameters and give a brief account of the Quark-Nova (henceforth QN) and the relativistic ejecta it produces. In §3, we describe characteristics of the circumbinary disk (CD). The interaction between the ejecta from the QN and the CD is studied in §4 where we describe the energetics and spectral features of the prompt emission. Using our model, we perform fits to observed GRBs that bring out the origin of the empirical Band function. We also derive the duration of the prompt emission in our model and predict an optical counterpart. Extended emission arising from ablating the white dwarf is addressed in §5. Late X-ray activity ascribed to the spin-down evolution of the quark star and accretion from trapped debris is explained in §6 along with afterglows from the shocked CD. §7 contains our main conclusions.

2. QUARK-NOVA IN A NS-WD LMXB

Staff et al. (2006), using standard equations of state (EOS) of neutron-rich matter, considered the likely NS candidates that could reach quark deconfinement density in their core; the fiducial value was taken to be $\sim 5\rho_0$, where $\rho_0 \sim 2.7 \times 10^{14} \text{g/cc}$ is nuclear saturation density. To reach $\sim 5\rho_0$, a NS with gravitational mass $M_G \sim 1.8M_\odot$ (using the APR EOS; Akmal et al. (1998)) is required.

Quark deconfinement in the core of the NS can happen in two ways: (i) right after the neutron star is formed, if the above criteria is satisfied. This is not relevant to the model presented, but could be important for superluminous supernovae (Ouyed et al. (2009, 2010)); (ii) If the above criteria is not met, the neutron star can accrete mass from a companion and reach the critical mass for deconfinement and subsequent QN explosion. This is the scenario considered in our model.

2.1. The LMXB evolution

We begin with the standard LMXB evolution model (Verbunt 1993), where a system with a relatively long orbital period (~ 1 day) produces a recycled pulsar when the subgiant progenitor of the white dwarf overflows its Roche lobe. In the first accretion phase, mass and angular momentum losses shorten the orbital period. Once this first accretion phase ceases, the orbital period continues to decay due to gravitational wave radiation. Eventually, the orbit decays enough for the white dwarf itself to overflow its Roche lobe, commencing the second, ultrashort orbital period (< 1 hr) LMXB phase. Here we are mainly concerned with the first recycling phase.

The orbital separation of the binary, a , evolves according to Kepler's third law

$$a = 2.28 \times 10^9 \text{ cm } (1+q)^{1/3} \left(\frac{M_T}{M_\odot} \right)^{1/3} \left(\frac{P_{\text{orb.}}}{60 \text{ s}} \right)^{2/3}, \quad (1)$$

where $q = M_{\text{WD}}/M_{\text{NS}}$, and $M_T = M_{\text{NS}} + M_{\text{WD}}$ the total mass of the system. The mass of the WD, M_{WD} , is constrained by the expected core mass of the Roche Lobe filling progenitor in the LMXB phase, $M_{\text{WD}} \sim 0.15M_\odot$. We adopt $M_{\text{WD}} \sim 0.1M_\odot$ representing the WD's fiducial value near the end of the first accretion phase. We will make use of the WD mass-radius relation (Savonije

(1983))

$$\frac{R_{\text{WD}}}{R_{\odot}} = 0.028(1 + X)^{5/3} M_{\text{WD},0.1}^{-1/3}, \quad (2)$$

with $M_{\text{WD},0.1}$ being the white dwarf mass in units of $0.1M_{\odot}$. Hereafter we take $X = 0$ (the Hydrogen fraction in the WD), since we assume a pure He WD near the end of the first accretion phase.

At the end of the first recycling process (i.e. first accretion phase), the neutron star will reach an equilibrium period (Bhattacharya & van den Heuvel 1991) which is approximated by the Keplerian orbital period at the Alfvén radius (Ghosh & Lamb 1992):

$$P_{\text{NS,eq.}} \sim 2 \text{ ms } B_{\text{NS},9}^{6/7} R_{\text{NS},6}^{16/7} M_{\text{NS},1.4}^{-5/7} \dot{m}_{\text{NS,Edd}}^{-3/7}, \quad (3)$$

where $B_{\text{NS},9}$, $R_{\text{NS},6}$ and $M_{\text{NS},1.4}$ are the neutron star surface magnetic dipole field, radius and mass in units of 10^9 G, 10^6 cm and 1.4 solar mass respectively. The accretion rate onto the neutron star, \dot{m}_{NS} , is given in units of the Eddington limited accretion rate $\dot{M}_{\text{Edd}} \sim 10^{-8} M_{\odot} \text{ yr}^{-1}$ above which the radiation pressure generated by accretion will stop the accretion flow.

Neutron stars as massive as $\sim 1.8M_{\odot}$ are not easy to produce in LMXBs even for initially high mass of the donor star, unless they were already born as relatively massive neutron stars (e.g. Lin et al. (2010)). Assuming up to $\sim 0.2M_{\odot}$ can be accreted (which will spin-up the NS to millisecond periods)¹ by the end of the first accretion phase, this puts a constraint on the minimum mass of the NS at birth of $\sim 1.6M_{\odot}$. Therefore a prolonged phase of accretion at the Eddington rate for $> 10^7$ years is needed. Thus LMXBs with NSs born massive and accreting near the Eddington limit are the most likely systems to experience a QN explosion near the end of the first recycling phase. Figure 1 (upper panel) is a schematic representation of the LMXB system at the end of the first accretion phase just before the QN goes off.

2.2. The Quark-Nova

In the Quark-nova picture (Ouyed et al. 2002), there is an explosive phase transition to the more compact (u, d, s) quark phase, and the gravitational potential energy is released partly into outward propagating shock waves from the supersonic motion of the (u, d, s) conversion front. The temperature of the quark core thus formed rises quickly to 10-20 MeV since the collapse is adiabatic rather than isothermal (Gentile et al. 1993). As mentioned in the introduction, a complete dynamical treatment of the QN, including multi-dimensional neutrino transport and hydrodynamics is only in the preliminary stages (Niebergal et al. 2010b) but results based on calculations incorporating the most physics suggest that a detonation is possible. The important outcome of the QN, as we now explain, is that chunks of the neutron star's crustal matter, rich in iron-group elements, can be ejected from the surface of the neutron star at relativistic speeds.

¹ The spin-up of a slowly rotating neutron star with moment of inertia I_{NS} to the equilibrium spin period $P_{\text{NS,eq.}} = 2\pi/\Omega \sim 2 \text{ ms}$ would require mass accretion of at least $\sim I_{\text{NS}}\Omega_{\text{NS}}/(GM_{\text{NS}}R_{\text{NS}})^{1/2} \sim 0.2M_{\odot}$ (Bhattacharya & van den Heuvel 1991).

2.3. The Quark-Nova ejecta

Unlike Supernovae, neutrino-driven mass ejection in Quark-novae is not feasible, as neutrinos are trapped inside a hot and dense expanding quark core, once it grows to more than $\sim 2 \text{ km}$ (Keränen et al. 2005). In (Keränen et al. 2005), we used a typical inelastic neutrino-nucleon cross-section to show that these (electron-) neutrinos are absorbed in the neutron-rich crust of the neutron star. The corresponding diffusion timescale out of the conversion front is ~ 0.1 seconds. Although the neutrinos have a similar luminosity as in supernovae (using the *per species* number for the latter), there is an important difference in the outcome for mass ejection. Unlike the case of a supernova, where neutrinos can drive a wind from the surface of the proto-neutron star, the neutron-rich crust is much too dense for these neutrinos to transfer kinetic energy effectively (the gravitational potential well is much deeper). Rather, they heat up the crust to temperatures of $\sim 1 \text{ MeV}$. In comparison to the photon-driven explosion (Vogt et al. 2004) which we have invoked here, energy deposition by neutrinos is less than 10% of the total energy budget. Therefore, it is not expected to lead to much baryon-loading of the photon fireball. Mass ejection due to core bounce is also unlikely unless the quark core is very compact (1-2) km. A more promising alternative is mass ejection from an expanding thermal fireball that is a direct consequence of dense, hot quark matter produced as a result of the conversion from neutron matter (Vogt et al. 2004; Ouyed et al. 2010). The fact that more than 50% of the gravitational and conversion energy is released as photons is unique to the QN (Ouyed et al. 2005). It allows for ejecta with kinetic energy easily exceeding 10^{52} ergs. Depending on the conversion efficiency of photon energy to kinetic energy of the ejecta (the neutron star's outermost layers), up to $10^{-2}M_{\odot}$ of neutron-rich material can be ejected at nearly relativistic speeds. Calculations of mass ejection in the QN scenario accounting for energy transfer to the crust, give estimates of ejected mass of $10^{-5}M_{\odot}$ - $10^{-2}M_{\odot}$ (Keränen et al. 2005). The average Lorentz factor of the QN ejecta is,

$$\Gamma_{\text{QN}} = \frac{\eta E_{\text{QN}}}{M_{\text{QN}} c^2} \sim 10 \frac{E_{\text{QN},52}^{\text{KE}}}{M_{\text{QN},-3.3}}, \quad (4)$$

where $E_{\text{QN},52}^{\text{KE}} = \eta_{0.1} E_{\text{QN},53}$ is the kinetic energy of the ejecta in units of 10^{52} erg. Here $\eta \sim 0.1$ is the efficiency of energy transfer from the QN total energy ($\sim 10^{53}$ ergs from gravitational and phase conversion energy) to the ejecta's kinetic energy. The QN ejecta mass, $M_{\text{QN},-3.3}$ is given in units of $5 \times 10^{-4}M_{\odot}$ which we adopt as our fiducial value.

There are two main sources of uncertainty to calculating the Lorentz factor (the neutrino contribution, we have argued above, is not more than 10% and is unlikely to change much even with improved calculations of neutrino transport in dense matter). The first is the thermal-to-kinetic conversion efficiency η in eq.(4), which we have taken as 0.1 (e.g. Frank et al. (2002)). Fixing this number is equivalent to fixing the amount of mass ejected. We are at present working on reducing this uncertainty by numerical modeling of the hydrodynamics of the conversion (from neutron to quark matter) front, including particle diffusion and advective forces into account (see

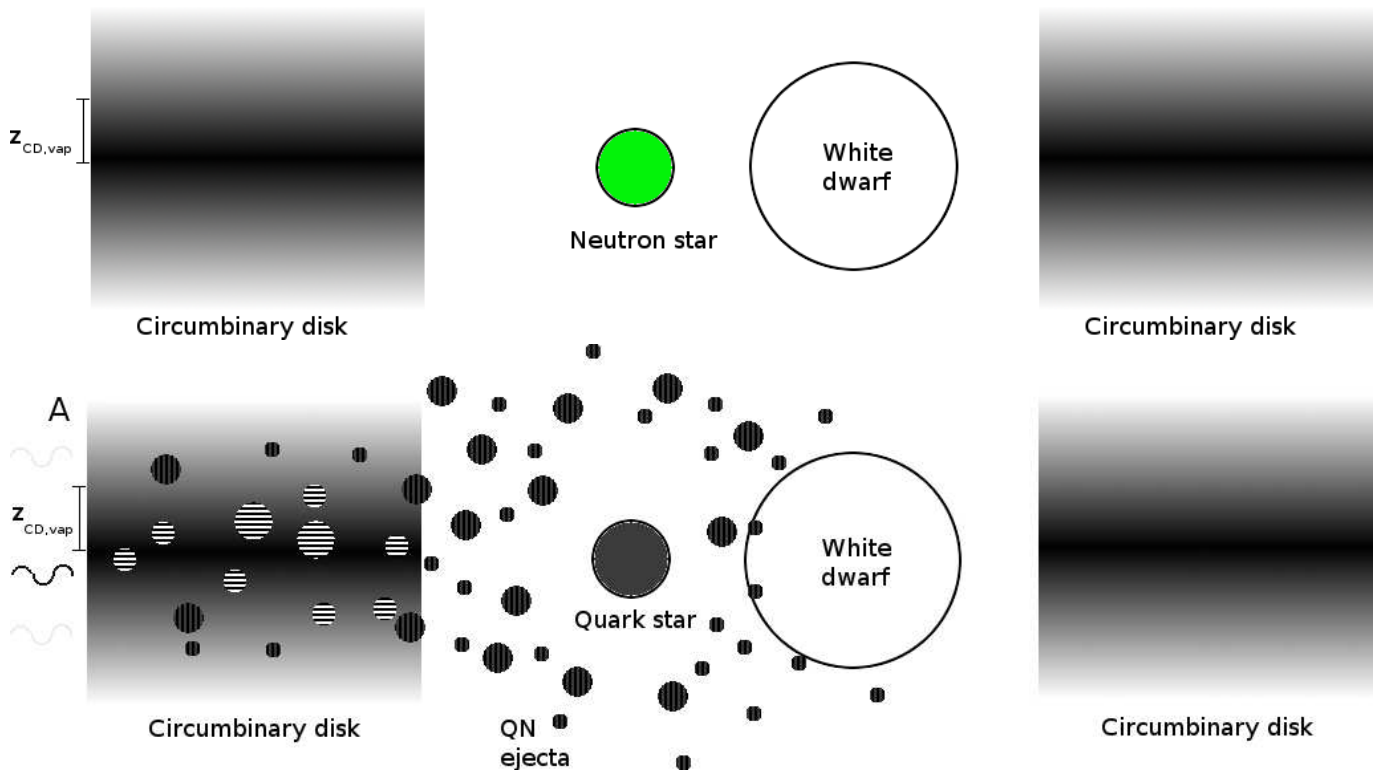


FIG. 1.— **Upper Panel:** A LMXB system which consists of a neutron star, a low mass white dwarf ($M_{WD} \sim 0.1M_{\odot}$ in our model) and a circumbinary disk near the end of the first accretion era. **Lower Panel:** Near the end of the first accretion phase, the neutron star experiences a QN explosion ejecting the neutron star crust and leaving behind a quark star. The QN chunks are ejected during the QN explosion hitting the circumbinary disk material at different latitudes. Below a critical height $z_{CD,vap}$ (from the midplane of the disk), the disk density is sufficiently high that the QN chunks are shocked above evaporation temperatures (circles with horizontal stripes). At heights greater than $z_{CD,vap}$ the density is low enough for the QN chunks to survive the shock and emit in the optical (circles with vertical stripes). A portion of the QN chunks will collide with the white dwarf causing it to partially or fully ablate, depending on the NS-WD separation and the white dwarf mass, when the QN explosion occurs.

Niebergal et al. 2010b). Once these simulations are extended beyond 1D, a comparison of the thermal energy density of the conversion front versus the pressure exerted on the surrounding matter should provide a better constraint on η .

The second source of uncertainty is the EoS and composition of the high density matter that is ejected. Our estimate for the fiducial value of ejected mass (and hence Γ_{QN}) is based upon a fit to the EoS of the neutron star crust, specifically the BPS equation of state for the outer crust (Baym et al. 1971) which is matched to a higher density equation of state for the inner crust. The equation of state for the outer crust is reasonably robust but can be improved by a few percent by taking into account more recent models based on quantum molecular dynamical (QMD) simulations of the nature of the crust post-accretion (eg. Horowitz & Kadau 2009); astrophysical phenomena such as quasi-periodic oscillations (QPOs) can also provide constraints (eg. Watts & Strohmayer 2007). The higher density of the inner crust is however poorly constrained, since it involves very neutron-rich nuclei and possibly some “pasta” phases. We expect that upcoming experiments with rare-isotope beams (eg. FRIB; <http://www.jinaweb.org/ria/>) will provide better constraints in the high-density regime.

Ouyed & Leahy (2009) studied the relativistically expanding shell of iron-rich ejecta emitted from the neutron star crust and found that it breaks up into numerous chunks because of lateral expansion forces (10^7 to 10^{11} chunks depending on whether the ejecta cools in the solid

or liquid phase). The typical chunk size at birth was calculated to be $\Delta r_{chunk,b} \sim 186 \text{ cm} \psi_{-3} r_{b,7} \rho_{b,8}$ where ψ is the iron breaking strain in units of 10^{-3} (the iron breaking strain is $\sim 10^{-3}$ for solid iron and ~ 0.1 for the liquid phase), $r_{b,7}$ is the radius in units of 10^7 cm when breaking starts and $\rho_{b,8}$ is the ejecta density in units of 10^8 g cm^{-3} at breakup (see §3.4 and Table 1 in Ouyed & Leahy 2009). The chunk’s rest length l_{chunk}^r is much larger than its width $\Delta r_{chunk,b} \sim 200 \text{ cm}$ for the solid phase (which we consider in this paper) or equal to its width for the liquid phase (Ouyed & Leahy 2009). In the solid case, the chunks thus resemble “iron needles” moving parallel to their long axis. In the observer’s frame the ratio of length to width will be contracted by $1/\Gamma_{QN}$.

Even beyond the break-up radius, the chunks remain in contact with each other within the relativistically expanding ejecta as a whole. This is because the pieces expand in volume, filling up the space between them, and causing the density of each piece to continuously decrease, until they reach the zero pressure iron-density (ρ_{Fe}), at radius $r_{sep} \sim 2 \times 10^9 \text{ cm}$, at which point they stop expanding. From Ouyed & Leahy (2009), the typical chunk size at r_{sep} is $\Delta r_{chunk} \sim 10^5 \text{ cm}$ while its length is of the order of 10^6 cm for the solid ejecta case. As the chunks continue to expand radially outwards to a radius $r > r_{sep}$, we can associate with them a filling factor $f_{chunk} = r_{sep}^2/r^2$.

We will now motivate the statistical model of ejecta break-up. Investigations of the fragment-size distribu-

tion (FSD) that results from dynamic brittle fragmentation show that fragmentation is initiated by random nucleation of cracks that are unstable against side-branch formation (Åström et al. 2004). The initial cracks and side branches individually form an exponential and a scale invariant contribution, respectively. Both merge to yield the resulting fragment size distribution which is expressed in the general form $n(s) \propto s^{-\alpha} f_1(s/s_1)$ with $\alpha = (2D - 1)/D$ (D being the Euclidean dimension of the space), f_1 a scaling function (an exponential) that is independent of s_1 for fragments smaller than s_1 and decays rapidly for $s > s_1$ (Åström 2006). Here $s_1 = \lambda^D$ where λ is the penetration depth of a branching crack. Adopting this model, the emergent picture for the relativistically expanding shell of QN ejecta is as follows: cracks are initially nucleated at random and more or less uncorrelated locations. From these locations, cracks propagate in different directions. The main cracks form large fragments with an exponential Poisson distribution with a typical size determined by Δr_{chunk} . The size (i.e. mass) of the Poisson-process fragments will be limited or reduced by the creation of small-size fragments (s_1) around each crack by the side-branching process. The final fragment size distribution becomes (Åström 2006):

$$n(s) = (1 - \beta) \left(\frac{s}{s_0} \right)^{-\frac{2D-1}{D}} \exp \left(-2^D \frac{s}{s_0} \right) + \beta \exp \left[-\frac{(s^{1/D} + s_0^{1/D})^D}{s_0} \right], \quad (5)$$

where $s_0 = \Delta r_{\text{chunk}}$ in our model.

Theoretical and experimental investigations (Sharon et al. 1995; Sharon & Fineberg 1996) have shown that a dynamic instability controls a crack's advance when its velocity exceeds a critical velocity of $0.36v_R$ where v_R is the Rayleigh wave speed in the material (a Rayleigh wave is a surface acoustic wave that travels on solids). Beyond $0.36v_R$ the mean acceleration of the crack dynamics change dramatically. At that point, the mean acceleration of the crack drops, the crack velocity starts to oscillate leading to the so-called Yoffe instability (Yoffe 1951) which leads to side-branching (e.g. Buehler & Gao 2006). Numerical solutions of the model for $v > 0.36v_R$ exhibit the occurrence of these branching events where the main crack sprouts side branches. The spacing between these branches is a function of the amount of dissipation. The above equation assumes that crack branches propagate easily with large penetration depth given by $\lambda = \Delta r_{\text{chunk}}^{1/D}$. Shown in Figure 2 is the FSD for two-dimensional fragmentation with $D = 2$ (i.e. $\alpha = 1.5$)². There are two natural scales in our model, the typical fragment scale Δr_{chunk} (and thus mass m_{chunk}) and, the scale at which the two terms/contributions in the RHS of

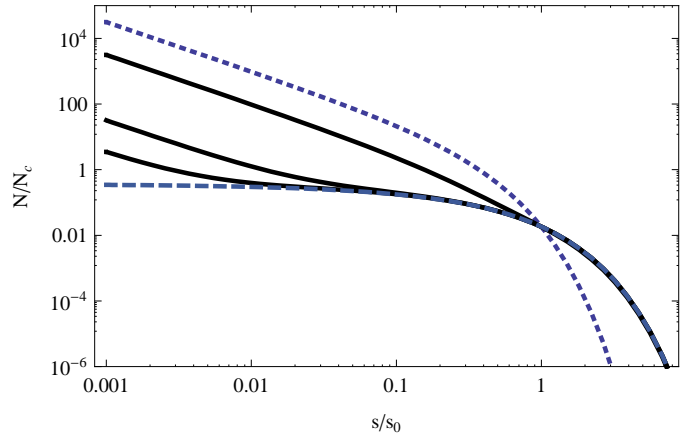


FIG. 2.— Log-Log plot of the Quark-Nova normalized fragments size distribution for $D = 2$. The dotted top curve is for $\beta=0$ (chunk distribution is purely defined by the main cracks) while the dashed bottom curve is for $\beta=1$ (chunk distribution is purely defined by the branching cracks). The three solid curves, from top to bottom, are for $\beta = 0.9, 0.99, 0.999$ and illustrate the contribution from the two size distributions as described in equation (5).

equation (5) are equal, which we call, Δr_t . For $s < \Delta r_t$ FSD is dominated by the side branching. As can be seen in Figure 2 the transition size becomes smaller, i.e. $m_t/m_{\text{chunk}} \ll 1$ as $\beta \rightarrow 1$. As we show later in §4.1, this statistical model plays a key role in explaining the empirically observed Band function of GRB spectra (Band et al. (1993)).

3. THE CIRCUMBINARY DISK

Circumbinary disks (CDs) could accompany the formation and evolution of binaries. These CDs are either the remains of fallback disks produced in the supernovae that formed the compact object (e.g. Wang et al. 2006; Cordes & Shannon 2008), or material injected into circumbinary orbits during the process of mass loss by the Roche lobe-filling companions (Dubus et al. 2002). The possibility that the CB disk is the remnant of the common envelope evolution phase of binaries cannot be ruled out either. Due to the tiny CD mass that would result, even after billions of years, such disks would be difficult to detect in the optical and infrared. Nevertheless, the detection of excess mid-infrared flux in few LMXBs in quiescence suggests that dusty circumbinary material might be present around some LMXBs (Muno & Mauerhan 2006) (see also Bowler (2010)). This remains to be confirmed. Here we consider (and assume) the case in which the binary system is surrounded by stable circumbinary disk/material continuously replenished during the process of (near-Eddington) accretion. As we have said, building massive NSs in LMXBs would require near Eddington accretion rates. This, we argue, could favor the formation and the sustainment of the CD.

There are different possible configurations for the CD such as a flat or flared disk. Here, we assume the replenished disk to be a geometrically thin, viscous Keplerian circumbinary disk. Its scale height, H_{in} , at the inner edge, R_{in} , is $H_{\text{in}} \sim 0.03R_{\text{in}}$ (Belle et al. 2004). The disks could lie as close to the center of mass of the binaries as $R_{\text{in}} \simeq 1.7a$, at which point they would be tidally truncated (Taam et al. 2003; Dubus et al. 2004). The dependence of the vertically integrated surface mass den-

² A special case is, however, when a two-dimensional object (i.e. a thin plate and/or closed shells) is fragmented in a three-dimensional space. Models revealed that the branching-merging picture for two-dimensional fragmentation may be valid for the initial stages of fragmentation, but fragmentation may continue as a cascade of breakups beyond the limit of maximum fragmentation through branching and merging of cracks. It was found that at later stages additional fragments were formed with a power-law FSD that had $\alpha \sim 1.17$ (Linna et al. 2004).

sity, Σ on radius R , is taken from (Taam & Spruit 2001), particularly Figure 8 in that paper, from which one can approximate $\Sigma \sim \Sigma_{\text{in}}(R_{\text{in}}/R)$. The mass of the disk is then

$$M_{\text{CD}} = \int_{R_{\text{in}}}^{R_{\text{out}}} \Sigma(R) R dR \sim \Sigma_{\text{in}} R_{\text{in}}^2 (R_{\text{out}}/R_{\text{in}} - 1) \quad (6)$$

$$\simeq 1.5 \times 10^{-6} M_{\odot} \Sigma_{\text{in},5} a_{10}^2 \zeta_{\text{CD,out}}$$

where $\zeta_{\text{CD,out}} = (R_{\text{out},12}/R_{\text{in},10} - 1)$. For a disk that is vertically isothermal, at a given radius R , the equation of hydrostatic equilibrium combined with the radial profile above yields (Belle et al. 2004):

$$\rho_{\text{CD}} = \frac{\Sigma_{\text{in}}}{H\sqrt{2\pi}} \left(\frac{R_{\text{in}}}{R} \right) \exp \left(-\frac{z^2}{2H_{\text{CD}}^2} \right). \quad (7)$$

Unlike a Shakura-Sunyaev disk, in CDs, the opening angle, H/R , is expected to be roughly constant (here ~ 0.03). Recalling that $R_{\text{in}} \simeq 1.7a$, the above then yields

$$\rho_{\text{CD}} \sim \rho_{\text{in}} \left(\frac{R_{\text{in}}}{R} \right)^2 \exp \left(-\frac{z^2}{2H_{\text{CD}}^2} \right), \quad (8)$$

where $\rho_{\text{in}} \sim 10^{-4} \text{ g cm}^{-3}$ ($\Sigma_{\text{in},5}/a_{10}$) and $\Sigma_{\text{in},5} = \Sigma_{\text{in}}/10^5 \text{ g cm}^2$. The column density as seen at a viewing angle $90^\circ - i = \theta_{\text{view}} = z_{\text{view}}/R$, where i is the inclination angle of the system is

$$N_{\text{CD}} = \frac{1}{\mu_{\text{CD}} m_H} \int_{R_{\text{in}}}^R \rho_{\text{CD}} dR \quad (9)$$

$$\sim 6 \times 10^{29} \Sigma_5 \exp \left(-\frac{\theta_{\text{view}}^2}{2\theta_c^2} \right),$$

where m_H is the proton mass and $\mu_{\text{CD}} \sim 1.2$ is the mean molecular weight for the CD material which we assume has a solar composition.

4. PROMPT EMISSION

We first address the fate of the QN chunks when they impact the CD. The chunks shock the CD material, and in turn, undergo a reverse shock that heats them to a temperature found from pressure balance $P_{\text{chunk}} = P_{\text{CD,sh.}}$. The pressure in the shocked CD material, $P_{\text{CD,sh.}}$, is found from the jump conditions (Russo 1988; Iwamoto 1989). We get, at $R = R_{\text{in}}$,

$$k_B T_{\text{chunk}} \sim 30 \text{ keV} \frac{\Sigma_{\text{in},5} \Gamma_{\text{QN},10}^2}{a_{10}} \exp \left(-\frac{z^2}{2H_{\text{in}}^2} \right). \quad (10)$$

Noting that non-degenerate iron will vaporize if heated to $\geq 0.3 \text{ eV}$ (CRC-Press 2005, for vaporization temperature of iron at normal density), the rapid fall-off of the CD density given by eq.(8) implies that the vaporization is already efficiently accomplished by interaction with the inner edge of the disk. At the inner edge of the CD, we can define a critical disk height, $z_{\text{CD,vap.}}$ (and corresponding density $\rho_{\text{CD,vap.}}$), below which the chunks will start vaporizing upon impact (see Fig. 1 for a schematic illustration of the process). This critical height is $z_{\text{CD,vap.}} \sim 4.8 H_{\text{in}}$ with a corresponding CD density $\rho_{\text{CD,vap.}} \sim 5.8 \times 10^{-7} \text{ g cm}^{-3}$. It follows that

the solid angle extended by the critical surface defined by $\rho > \rho_{\text{CD,vap.}}$ is then

$$\Omega_c = \frac{2\pi R_{\text{in}} 2z_{\text{CD,vap.}}}{4\pi R_{\text{in}}^2} \sim 4.8 \frac{H_{\text{in}}}{R_{\text{in}}} \sim 0.15. \quad (11)$$

The amount of QN ejecta material contained within Ω_c is $M_{\text{QN,c}} = \Omega_c M_{\text{QN}} \simeq 7.5 \times 10^{-5} M_{\odot} M_{\text{QN},-3.3}$.

The time it takes a given chunk to be completely eroded is

$$t_{\text{vap.}} = \frac{l_{\text{chunk}}^r}{2v_s \Gamma_{\text{QN}}^2} \sim 4.3 \times 10^{-6} \text{ s} \frac{l_{\text{chunk},5}^r a_{10}^{1/2}}{\Sigma_{\text{in},5}^{1/2} \Gamma_{\text{QN},10}^3}, \quad (12)$$

where $v_s = \sqrt{(k_B T_c / 2m_H)}$ is the speed at which the heat wave crosses the chunk. The chunk's Thompson optical depth, $\sim 1/(n_{\text{chunk}} \sigma_T)$, is much less than the typical chunk size, $\Delta r_{\text{chunk}} \sim 10^5 \text{ cm}$ (the chunk's density is about $\sim 10^3 \text{ g cm}^{-3}$ by the time they reach the CD; see §5). During their extremely brief life as solid entities in the CD, most of the chunks will emit as blackbodies at a rate $L_{\text{chunk}} = A_{\text{chunk}} \sigma T_{\text{chunk}}^4$ where $A_{\text{chunk}} \sim \pi \Delta r_{\text{chunk}}^2$. For a typical chunk, $L_{\text{chunk}} \sim 10^{40} \text{ erg s}^{-1} T_{c,30}^4$ where the chunk's temperature is given in units of 30 keV. The total luminosity in blackbody emission can be estimated by recalling that the total area extended by the chunks is $\sim 4\pi a^2$ so that $L_{\text{BB}} \sim \Omega_c 4\pi a^2 \sigma T_c^4 \sim 10^{49} \text{ erg s}^{-1} T_{c,30}^4$. The corresponding isotropic blackbody contribution from all the chunks is $L_{\text{BB,iso.}} = L_{\text{BB}}/\Omega_c \sim 10^{50} \text{ erg s}^{-1}$. An observer would see a blackbody peaking at $\Gamma_{\text{QN}} T_{\text{chunk}}$.

A given chunk will continue to plow CD material even after complete vaporization and erosion since the vaporized material will retain the directional motion and size distribution of the incoming chunks. The vaporized chunk material will eventually enter a deceleration phase once it plows a mass of $\sim m_{\text{chunk}}/\Gamma_{\text{QN}}$ (e.g. Rhoads 1997) in CD material. This puts a constraint on the minimum mass of the CD disk necessary to stop the QN ejecta within Ω_c . It is $M_{\text{CD,min}} = M_{\text{QN,c}}/\Gamma_{\text{QN}} \sim 7.5 \times 10^{-6} M_{\odot} M_{\text{QN},-3.3}$. In our model, this translates to a minimum disk size $R_{\text{out,min}} = R_{\text{stop}}$ given by $\zeta_{\text{CD,stop}} \simeq R_{\text{stop}}/R_{\text{in}} \sim 500 M_{\text{QN},-3.3}/(\Sigma_{\text{in},5} a_{10}^2 \Gamma_{\text{QN},10})$. This critical radius is important for the kinematics and dynamics of a given chunk in the CD. Assuming a CD with $R_{\text{out}} > R_{\text{stop}}$ implies that most of the vaporized QN ejecta will lose its momentum and kinetic energy to the CD material before it reaches the outer edge of the disk (see §4.2).

4.1. Spectrum: Origin of the Band Function

For the prompt emission, we isolate two broad regimes (in addition to the blackbody emission from the heated chunks) in our model depending on whether the shock temperature of the chunks exceeds the nuclear dissociation temperature (binding energy) for iron or not.

4.1.1. Regime 1 - MeV photons, transient Fe lines

Upon impact, the chunks are heated to temperatures above 0.3 eV but below 8.8 MeV, in which case they vaporize without dissociation. Prompt emission in our model is tied to the shocked CD material, whose temperature $T_{\text{CD,s}}$ can be estimated as follows: The chunk plows through the CD while vaporizing into a hot stream

of gaseous particles which retain the directional motion of the incoming chunks. In this case, in the observer's frame,

$$\frac{\rho_{\text{CD}}}{\rho_{\text{chunk}}^{\text{obs}}} \Gamma_{\text{QN}} m_{\text{chunk}} c^2 \sim \frac{dM_{\text{CD,plow}}}{\mu_{\text{CD}} m_H} k_B T_{\text{CD,s}}. \quad (13)$$

We have $dM_{\text{CD,plow}} = A_{\text{chunk}} \rho_{\text{CD}} dR_{\text{CD,obs}}$, where A_{chunk} is the area of the chunk and $dR_{\text{CD,obs}}$ is the distance traveled by the vaporized chunk as measured by an observer. The above equation is valid as long as $dM_{\text{CD,plow}} < m_{\text{chunk}}/\Gamma_{\text{QN}}$. The chunk's rest mass is $m_{\text{chunk}} = \rho_{\text{chunk}}^r A_{\text{chunk}} l_{\text{chunk}}^r$ with $\rho_{\text{chunk}}^{\text{obs}} = \Gamma_{\text{QN}} \rho_{\text{chunk}}^r$. Replacing in eqn.(13) yields

$$k_B T_{\text{CD,s}} \sim \mu_{\text{CD}} m_H c^2 \times \frac{l_{\text{chunk}}^r}{dR_{\text{CD,obs}}}. \quad (14)$$

A limit on the observed temperature is then,

$$k_B T_{\text{CD,s}} > 10 \text{ keV } \mu_{\text{CD}} \times \frac{l_{\text{chunk},5}^r}{dR_{\text{CD,obs},10}}, \quad (15)$$

where $dR_{\text{CD,obs}} \sim c \times dt \approx 10^{10} \text{ cm}$ to account for a typical GRB duration $dt_{\text{GRB}} \sim 0.3 \text{ s}$ (see §4.3). The temperature given above is the peak temperature after the chunk has plowed through most of the CD. Higher peak temperatures occur in the early stages of the plowing process.

Eqn.(14) is illuminating - it implies a direct proportion between the temperature of the shocked material and the linear size of the chunk. Since the linear size is distributed according to Eqn.(5), the temperature of the shocked CD material will also display the same distribution.

It is interesting to note that several GRBs show spectra (more precisely, $\nu F(\nu)$ curves) that appear to follow a log-normal distribution (Band et al. 1993). According to Brown&Wohletz (1995), fragmentation of a massive object that proceeds by formation and branching of cracks results in a distribution of masses (per unit logarithm in mass) that follows the Weibull distribution (Weibull 1939), which looks almost identical to the log-normal distribution. The Weibull distribution in mass can be written as (Brown&Wohletz 1995)

$$m^2 n(m) = N m_1 \left(\frac{m}{m_1} \right)^{\delta+2} \exp \left[-\frac{(m/m_1)^{\delta+1}}{\delta+1} \right] \quad (16)$$

where $\delta = -D/3$ is a fractal dimension and m_1 a mass related to the average fragment mass in the distribution. The peak of the distribution (called the most probable mass; in our case m_{chunk}) is given by $m_{\text{peak}}/m_1 = (2 + \delta)^{\frac{1}{1+\delta}}$; N is a normalization factor related to the total number of fragments. Note the formal similarity to the first term in eqn.(5), derived by Åström (2006), who based his expression on a more complicated fragmentation situation involving the competition between side-branching and cracking, which leads to the second term in eqn.(5).

Therefore, we put forward the intriguing suggestion that the GRB spectrum arises due to photons from the shock-heated CD material whose temperature distribution is inherited from a fragmentation distribution of the

QN ejecta. We assume a one-to-one relationship between the temperature of the shocked CD material and the resulting radiation energy; in this case, the prompt photon energy E_γ will inherit the fragmentation distribution. Although a full calculation of the non-thermal spectrum of the photons is beyond the scope of this work, we test this idea by performing fits to some observed GRB spectra by assuming that the photon luminosity ($\nu F(\nu) = E_\gamma^2 n(E_\gamma)$) follows the Weibull distribution given by (16),

$$E_\gamma^2 n(E_\gamma) = A_\gamma \left(\frac{E_\gamma}{E_0} \right)^{\delta+2} \exp \left[-\frac{(E_\gamma/E_0)^{\delta+1}}{\delta+1} \right] \quad (17)$$

where A_γ is a normalization factor and E_0 the average photon energy in the distribution. The peak of the distribution occurs at

$$E_{\text{peak}} = (2 + \delta)^{\frac{1}{1+\delta}} E_0. \quad (18)$$

In our model, the assumed one-to-one correspondence between $T_{\text{CD,s}}$ and E_γ implies that E_{peak} evolution in time is given by eq.(14). The fits to GRB 000218, GRB 000727, and GRB 980706A are shown in Figures 3&4. In reality the spectrum evolution will be related not just to the chunk distribution but also the vaporization rate. We expect the softening of the spectrum to be caused mostly by the erosion of the fast moving chunks which will be heated the most and thus radiate the most. The total number of chunks should also decrease in time with smaller chunks most likely disappearing (i.e. fully eroded) first. The case of GRB 000727 is an interesting one since its observed E_0 increases in time. However note the data is for shorter integration times than for the other two candidates (see Table 1). In our model, there is a minimum accumulation time (presumably of the order of milliseconds) before the full mass distribution (i.e. the Band spectrum) builds up. The excellent fits suggest that the underlying physical picture relating the spectrum to the ejecta fragment size or mass distribution is probably correct. In reality, the fragmentation process may be more complicated (e.g. eq.(5)), but the Weibull distribution appears to be an excellent approximation.

There are specific predictions for this component within our model: (i) The peak photon energy (related to l_{chunk}^r) should evolve in time according to equation (14); (ii) The prompt emission is composed of contributions from $\sim 10^7$ - 10^{11} "blobs" of emitting CD material plowed and heated by the relativistic vaporized chunks material. A given pulse in our model consists of different "blobs" of heated CD material emitting simultaneously. Thus a pulse should also carry the signature of the distribution in mass of the chunks (i.e. the Band function); (iii) finally, the prompt emission (regime 1) should have signatures of iron-group elements (Fe, Co, Ni) brought in by the chunks, but this should be transient since the vaporized material will cool rapidly.

4.1.2. Regime 2 - GeV photons, no Fe lines

Chunks heated above 8.8 MeV will be dissociated into nucleons and lose their identity by mixing with the CD matter. From Eqn.(10), this regime could occur for systems with $\Gamma_{\text{QN}} > 100$ (i.e. with $M_{\text{QN}} < 5 \times 10^{-5} M_\odot$).

The mixed CD and QN material will have a common temperature and will have some neutron excess (since

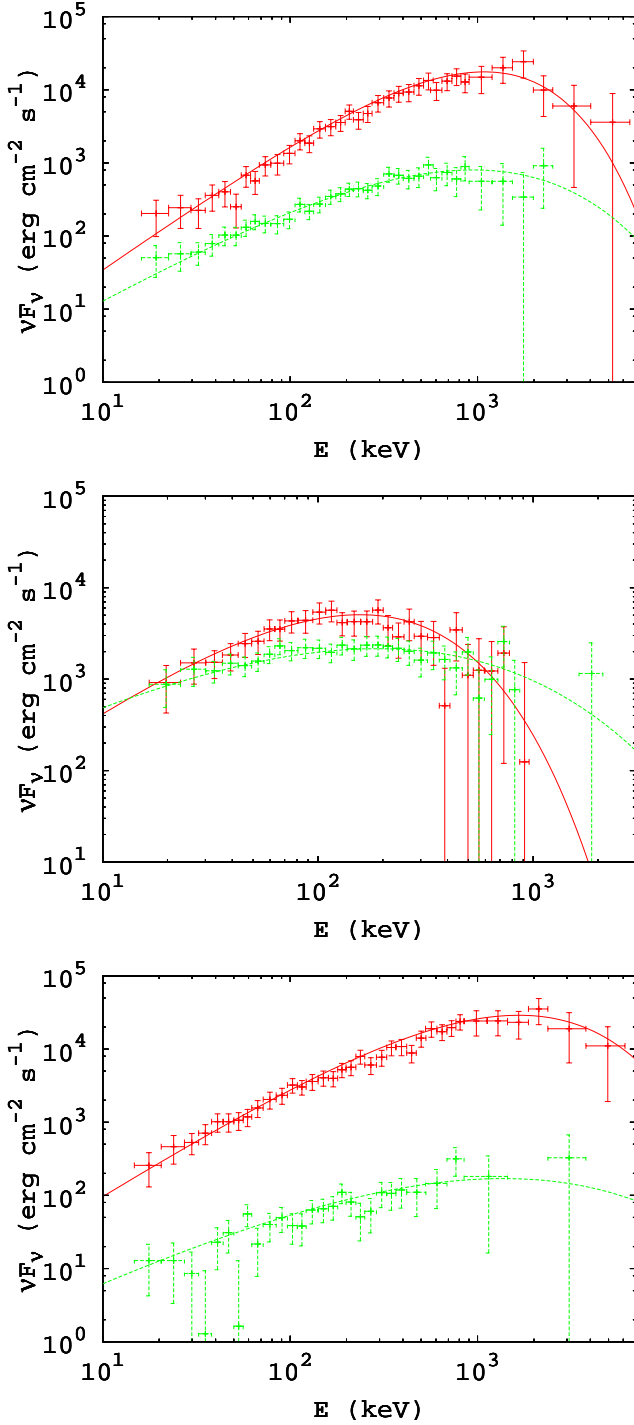


FIG. 3.— Model fit (solid curves) to observed photon spectrum (νF_ν) with data from Mazets et al. (2004) for GRB 000218 (top panel), GRB 000727 (middle panel), and GRB 980706A (bottom panel). The top and bottom data points, in each panel, are for different integration time (see Table 1).

the QN ejecta inherits its composition from the neutron star crust) with a mean molecular weight $\mu \sim 1$. We expect a given chunk to instantly transfer a significant fraction of its kinetic energy into heating $m_{\text{chunk}}/\Gamma_{\text{QN}}$ of CD material. The resulting thermal energy *per nucleon* is then

$$k_B T_{\text{nucl.}} \sim 100 \text{ GeV } \Gamma_{\text{QN},10}^2. \quad (19)$$

For such energies which exceed the threshold for pion

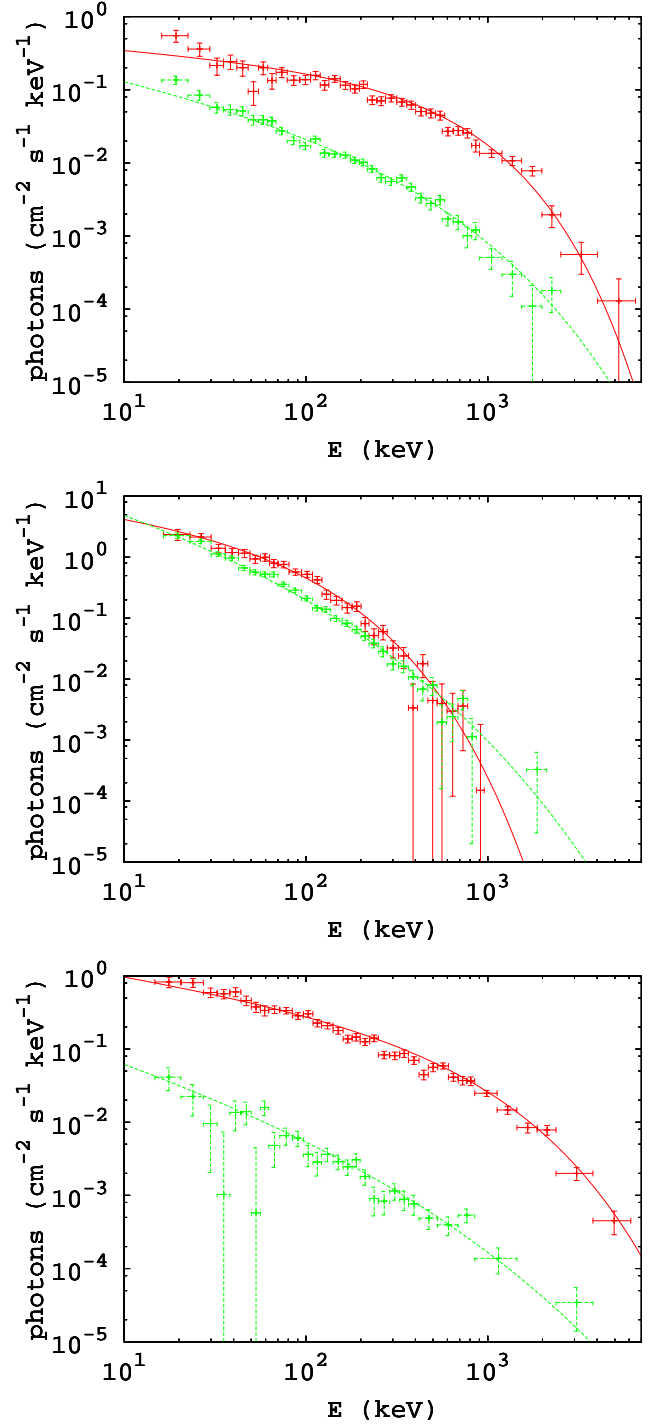


FIG. 4.— Model fit (solid curves) to observed photon flux $n(E_\gamma)$ with data from Mazets et al. (2004) for GRB 000218 (top panel), GRB 000727 (middle panel), and GRB 980706A (bottom panel). The top and bottom data points, in each panel, are for different integration time (see Table 1).

production, processes such as $p + p \rightarrow p + p + \pi^0$, $n + p \rightarrow p + p + \pi^-$, $p + p \rightarrow p + n + \pi^+$ can occur. Charged pion decay produces electrons and positrons which can annihilate to form photons, and neutron pions can produce photons by $\pi^0 \rightarrow 2\gamma$. The luminosity can be estimated from

$$L \sim \langle E_\pi \rangle \frac{\rho_{\text{chunk}} \rho_{\text{CD}}}{m_H^2} 2\pi R_{\text{in}} H_{\text{CD}} l_{\text{chunk}} c \sigma_{pp} \quad (20)$$

TABLE 1
MODEL FITS TO OBSERVED PHOTON SPECTRUM (GRB 000218, GRB 000727, AND GRB 980706A) USING EQ.(17). THE FITS ARE PERFORMED FOR OBSERVATIONS AT TWO DIFFERENT INTEGRATION TIME, $t_{\text{int.}}$.

GRB	$t_{\text{int.}}$	δ	E_0 (keV)	E_{peak}/E_0	A_γ
000218	0-256 ms	-0.2	520	2.1	0.164
	256 ms-5.888 s	-0.5	420	2.3	0.027
000727	0-128 ms	-0.33	73	2.2	3.2
	256 ms-768 ms	-0.65	80	2.4	5.0
980706A	0-256 ms	-0.39	760	2.2	0.2
	256 ms-8.448 s	-0.67	580	2.4	0.009

$$\sim 2 \times 10^{49} \text{ ergs/s } \Sigma_{\text{in},5} l_{\text{chunk},5} a_{10}$$

where we have assumed a typical cross-section for pp collisions in the tens of GeV range of $\sigma_{pp} \sim 10^{-25} \text{ cm}^2$ (i.e. 100 millibarns, Blattnig et al. 2000) and a typical pion energy $\langle E_\pi \rangle \sim 150 \text{ MeV}$ (threshold production).

We offer specific predictions for this high-energy component within our model: (i) We expect this component also to show traces of the chunk size distribution and partly follow a log-normal-like distribution. However, chunks heated to extreme temperatures ($>> 1 \text{ GeV}$) will start to move away from the band function; (ii) it should have no signatures of Iron-group elements since the ejecta is dissociated completely to nucleons; (iii) GeV and higher energy photons should be observed only in systems with $\Gamma_{\text{QN}} > 100$.

For the two regimes isolated above, the CD material between photons and the observer must be optically thin. The radiation will scatter most off of free electrons in the ionized CD material. The Compton optical depth is $N_{\text{CD}} \sigma_{\text{C}} \sim 2.7 \times \Sigma_5 \exp(-\theta_{\text{view}}^2/2\theta_{\text{c}}^2)$ where $\sigma_{\text{C}} = (3/8)\sigma_{\text{T}} \ln(x)/x^2$ is the Compton cross-section, $\sigma_{\text{T}} = 6.652 \times 10^{-25} \text{ cm}^2$ the Thompson cross-section, and x is the ratio between the prompt photon energy and the electron rest-mass which is $\sim 1 \text{ GeV}/(m_e c^2) >> 1$. The shocked matter is therefore Compton-optically thin to the high-energy photons. For the low energy photon regime, the Thomson optical depth is too high and this should negatively affect the ability to see the shocked chunks or the shocked disk gas since the deposited energy should thermalize over the whole disk. The disk geometry and vertical scale height, in our model, is assumed to be the simplest with $H/R = \text{constant}$. However other disk configurations are possible, such as a CD with a flared surface; $H \propto R^{3/2}$. This is a great advantage since a large solid angle is available for the chunks to be able to plow at an angle into increasing smaller density and thus be able to radiate in the optically thin regime. Specifically, for such a flared disk/atmosphere most of the chunks would be flying through the larger volume of the disk/atmosphere so most energy would be deposited in the region that is dense enough to significantly slow the chunks. Up high in the flared disk/atmosphere region the density is so low that the chunks fly through unimpeded. In summary, a $H \propto R^{3/2}$ would make a large visible impact surface available with a a longer lived black body from the optically thick part and a short lived brighter part from flared region of the disk.

4.2. Energetics

The energy deposited by the QN ejecta (into $\sim M_{\text{QN},c}/\Gamma_{\text{QN}}$ of CD material) gives us an estimate of the prompt GRB emission. The total thermal energy produced which we assume to be roughly equal to the total GRB energy is $E_{\text{GRB}} \sim \Gamma_{\text{QN}} \times (M_{\text{QN},c}/\Gamma_{\text{QN}})c^2 \sim 1.5 \times 10^{50} \text{ erg } M_{\text{QN},-3.3}$ where we have used $M_{\text{QN},c} = \Omega_{\text{c}} M_{\text{QN}}$. The effective isotropic energy in our model is thus $E_{\text{GRB,iso.}} \sim E_{\text{GRB}}/\Omega_{\text{c}} \sim 10^{51} \text{ erg } M_{\text{QN},-3.3}$. Observed short GRBs also have $E_{\text{GRB,iso}}$ up to 10^{51} erg (Nakar 2007).

In our model, the disk only subtends an angle $\sim 15\%$ of the sky. Thus, at most $\sim 10^{51}$ ergs of the QN kinetic energy 10^{52} erg intersects the disk to be radiated. It was shown by (Zhang et al. 2007) that the radiative efficiency $(E_\gamma/(E_\gamma + E_K))$ could vary from a few percents to more than 90% depending on how the kinetic energy is calculated. These studies are based on key assumptions about (i) the unknown shock parameters; (ii) the required detailed afterglow modeling with its own limitation and (iii) assumes the fraction of the electron energy in the internal energy of the shock to be 10%. Nevertheless let us assume an efficiency of ~ 0.1 for short GRBs which is also the number derived in an independent study by (Berger 2007). A 10% radiative efficiency would imply an $E_\gamma \sim 10^{50} \text{ erg}$ in true energy release corresponding to an isotropic energy release of $E_{\gamma,\text{iso.}} \sim 10^{51} \text{ erg}$. This number could be higher for disks with higher solid angle (e.g. flared CDs) and/or for QN ejecta with higher kinetic energy.

4.3. Duration

In our model, emission duration is related to the time it takes the QN ejecta to be stopped by its interaction with the CD:

$$t_{\text{GRB}} \simeq \frac{(R_{\text{stop}} - R_{\text{in}})}{2c\Gamma_{\text{QN}}^2} \sim 1.4 \text{ s } \frac{M_{\text{QN},-3.3}}{\Sigma_{\text{in},5} a_{10} \Gamma_{\text{QN},10}^3}. \quad (21)$$

The time-variability can vary from microseconds to a fraction of a second depending on the number of chunks (out of the $\sim 10^7$ - 10^{11}) that emit simultaneously at a given time.

4.4. The optical counterpart

The QN chunks hitting the CD in regions where $\rho_{\text{CD}} < \rho_{\text{CD,vap.}}$ (i.e. at heights $z > z_{\text{CD,vap.}}$; see Fig. 1) will not be fully vaporized, nor do they expand significantly. Rather, they pass through the CD, effectively puncturing it. During this interaction the temperature of a QN chunk is determined by shock heating, and will not exceed $\sim 3 \text{ eV } \Gamma_{\text{QN},10}$ as seen by an observer; thus emission would be in the optical band. The observed optical emission is related to shock efficiency with emitted energy $E_{\text{Opt.}} \simeq (0.3 \text{ eV} \times M_{\text{QN,Opt.}}/(\mu_e m_{\text{H}})) \times \Gamma_{\text{QN}}^2 \sim 10^{41} \text{ ergs } \Gamma_{\text{QN},10}^2 M_{\text{QN},-3.3}$ where $\mu_e = 2$ is the mean weight per electron and $M_{\text{QN,Opt.}} = \Omega_{\text{Opt.}} M_{\text{QN}}$ with $\Omega_{\text{Opt.}} = (z_{\text{CD,Opt.}} - z_{\text{CD,vap.}})/R_{\text{in}} \sim 0.3 H_{\text{in}}/R_{\text{in}}$ with the maximum height $z_{\text{CD,Opt.}}$ is calculated from eq.(10) using the lower limit of the optical band. Our model predicts optical emission to appear simultaneously with the prompt emission since the chunks penetrate all regions of the disk at the same time. The optical and prompt emission are both composed of short pulses from the impact of the chunks striking the CD.

4.5. Afterglow activity

The innermost CD material acts as a buffer for the dissociated and pulverized chunks. The cross-sectional area of the chunks increases rapidly sweeping up more CD mass, which leads to a run-away process. As they expand, they start increasing the covering factor of the blast. If enough chunks get dissociated a covering/filling factor of unity would eventually be reached. Energy-Momentum conservation implies that the mixed ejecta is ejected with speed, v_f , given by

$$\beta_f \Gamma_f = \frac{\sqrt{\Gamma_{\text{QN}}^2 - 1}}{1 + \frac{M_{\text{CD}}}{M_{\text{QN},c}}} \sim \frac{M_{\text{QN},c}}{M_{\text{QN},c} + M_{\text{CD}}} \Gamma_{\text{QN}}, \quad (22)$$

where $\beta_f = v_f/c$. Depending on $M_{\text{QN},c}/M_{\text{CD}}$, the mixed ejecta resembles a massive shell which expands at mildly relativistic speeds. External shocks with the circumstellar matter will slow down further the mixed ejecta and should produce an afterglow, which could last for months. This is similar to afterglow activity in the internal-external shock model of GRBs (Piran 2001) except that the prompt emission is caused by the chunks rather than by internal shocks. Additional afterglow activity can also occur if the non-dissociated chunks interact with matter beyond the outer edge of the CD.

To summarize, the QN naturally provides the relativistic “bullets” required by some GRB models (Heinz&Begelman 1999; Umeda 2000). However, the surrounding environment and emission region is very different in our model. The interaction between the relativistic QN chunks and the CD (as well as the chunks’ composition) is the key to the successes of our model - the origin of the Band function, as well as energetics, variability and duration which are consistent with observations. The interaction between the QN chunks and the WD is another feature of our model which we explore next.

5. EXTENDED EMISSION

Thus far, we have focused on the interaction between the chunks of ejecta and the CD as a means to explain the prompt emission. We now investigate the interaction between the chunks and the WD. As we show below, the WD can be ablated by the highly energetic chunks, leading to properties reminiscent of the extended emission (EE) observed in some shGRBs. The density of the QN ejecta at a distance r from the point of explosion is given by eq.(B3) in Ouyed&Leahy (2009). A combination of mass conservation and thermal spreading of the QN ejecta thickness, Δr , gives $\rho_{\text{QN}} \sim 10^3 \text{ g cm}^{-3} \rho_{0,14} \times \Delta r_{0,4}/(r_{10}^{9/4} M_{\text{QN},-3.3}^{1/4})$ where the density at ejection point (the surface of the NS), ρ_0 , is given in units of $10^{14} \text{ g cm}^{-3}$ (for an $M_{\text{QN}} \sim 5 \times 10^{-4} M_\odot$ ejecta; Datta et al. 1995). The ejecta thickness at ejection is $\Delta r_0 \sim 10^4 \text{ cm}$ or $\Delta r_{0,4} \sim 1$ in units of 10^4 cm . The chunks’ density at the WD location ($r = a$) is then $\sim 10^3 \text{ g cm}^{-3} \rho_{0,14} \times \Delta r_{0,4}/(a_{10}^{9/4} M_{\text{QN},-3.3}^{1/4})$ which is of the order of the WD density $\rho_{\text{WD}} \sim 6.3 \times 10^3 \text{ g cm}^{-3} M_{\text{WD},0.1}^2$. We thus expect the QN induced shock to pass through the WD rather than flowing around since the “crushing

time” $\sim (R_{\text{WD}}/c) \times (\rho_{\text{WD}}/\rho_{\text{QN}})^{0.5} \sim (R_{\text{WD}}/c) \ll 1 \text{ s}$ (Klein et al. 1994). Thus it is reasonable to assume that all of the intercepted kinetic energy will go into heating, rather than shocking on and flowing around, the WD.

5.1. Energetics

The total thermal energy deposited by the chunks impacting the WD is $\Omega_{\text{WD}} E_{\text{QN}}^K$, given by

$$E_{\text{th}} \sim 9.3 \times 10^{49} \text{ erg } E_{\text{QN},52}^K M_{\text{WD},0.1}^{-2/3} a_{10}^{-2}, \quad (23)$$

where $\Omega_{\text{WD}} = R_{\text{WD}}^2/(4a^2)$ is the solid angle subtended by the WD. If E_{th} exceeds the gravitational binding energy of the WD

$$E_{\text{G,WD}} = GM_{\text{WD}}^2/R_{\text{WD}} \sim 1.4 \times 10^{48} \text{ erg } M_{\text{WD},0.1}^{7/3} \quad (24)$$

then the WD would be ablated as a result of the QN explosion. The condition above imposes a nearness restriction on the WD as

$$a < a_{\text{th.}} = 8.2 \times 10^{10} \text{ cm } \frac{(E_{\text{QN},52}^{KE})^{1/2}}{M_{\text{WD},0.1}^{3/2}}. \quad (25)$$

For systems with $a < a_{\text{th.}}$, one should observe both prompt and extended emission.

The temperature per nucleon of the ablated WD will be an important quantity that determines the spectrum of the extended emission. It can be estimated as

$$k_B T_{\text{WD}} \sim 133 \text{ keV } \frac{\mu_{\text{WD},4/3} E_{\text{QN},52}^{KE}}{a_{10}^2 M_{\text{WD},0.1}^{5/3}}, \quad (26)$$

where μ_{WD} is the mean molecular weight in units of 4/3 (for a pure Helium WD). This implies that WD material is ejected at speeds

$$V_{\text{th.,eject.}} \sim 3 \times 10^3 \text{ km s}^{-1} \frac{E_{\text{QN},52}^{KE 1/2}}{a_{10} M_{\text{WD},0.1}^{5/6}}, \quad (27)$$

5.2. Spectrum

Nuclear burning timescales are much shorter than dynamical timescales. Depending on T_{WD} , various nuclear burning processes are expected to take place. As for the case of prompt emission, we can isolate the following interesting regimes:

5.2.1. Regime 1: $T_{\text{WD}} > 0.26 \text{ MeV}$, *Ni production*

From equation (26), this temperature regime corresponds to

$$a_{10} < a_{\text{Ni}} = 0.7 \frac{\mu_{\text{WD},4/3}^{1/2} E_{\text{QN},52}^{KE 1/2}}{M_{\text{WD},0.1}^{5/6}}, \quad (28)$$

In this range, the WD temperature $T_{\text{WD}} \geq T_{\text{Si}} \sim 3 \times 10^9 \text{ K}$, the temperature for Silicon burning. As a result, α -burning can occur all the way up to Nickel-56. The sequence of α -burning from Helium through to Nickel will release on average 7-8 MeV per nucleon, resulting in an energy release $\sim 2 \times 10^{50} \times M_{\text{WD},0.1} \text{ erg}$, which is enough

for complete disruption of the WD. The processed nuclei are ejected at speeds $V_{\text{nuc.,ejec.}} \sim 2.1 \times 10^4 \text{ km s}^{-1}$. The high speeds and nuclear processing imply that one should observe in this regime

- Broad emission lines ($\sim V_{\text{nuc.,ejec.}}$) early in the spectrum.
- No Hydrogen or Helium lines, weak or no Silicon line.
- Calcium, Nickel and Iron group lines

The signature of a QN in such a binary system is then similar in some respects to what is observed in Type Ic supernovae.

5.2.2. *Regime 2: $50 \text{ keV} < T_{\text{WD}} < 0.26 \text{ MeV}$, Silicon production*

From equation (26), this condition corresponds to

$$a_{\text{Ni}} < a_{10} < a_{\text{Si}} = 1.6 \frac{\mu_{\text{WD},4}^{1/2} E_{\text{QN},52}^{\text{KE}}{}^{1/2}}{M_{\text{WD},0.1}^{5/6}}, \quad (29)$$

This is sufficient for Carbon-burning and Oxygen burning, but not enough for Silicon burning. The observational signature of a QN in such a system would be

- No Hydrogen or Helium lines
- Oxygen, Magnesium lines
- Strong Silicon line if Oxygen burning also occurs ($T \geq 10^9 \text{ K}$)

This is similar in some respects to Type Ia SNe except that no Nickel can be produced. However, the QN ejecta, if not completely destroyed on impact, will still display weak Fe group lines since it is Iron-rich. Thus, these lines can show up in the late-time spectra making it closely resemble the characteristics of a Type Ia SN.

5.2.3. *Regime 3: $8.6 \text{ keV} < T_{\text{WD}} < 50 \text{ keV}$, Oxygen production*

This is sufficient for Helium ignition but not for Carbon burning. From equation (26), this regime corresponds to

$$a_{\text{Si}} < a_{10} < a_{\text{O}} = 3.9 \frac{\mu_{\text{WD},4}^{1/2} E_{\text{QN},52}^{\text{KE}}{}^{1/2}}{M_{\text{WD},0.1}^{5/6}}, \quad (30)$$

The total nuclear energy released $\sim 1.8 \times 10^{50} \times M_{\text{WD},0.1} \text{ erg}$ is once again enough for complete disruption of the WD, but the processed nuclei are ejected at slower speeds $V_{\text{nuc.,ejec.}} \sim 1.3 \times 10^4 \text{ km s}^{-1}$. α -burning is the most important process here, so that nuclei O, Ne, Mg are likely to be synthesized. Since Silicon burning cannot happen, elements such as Calcium cannot be synthesized in such an explosion, but can be brought in by the QN ejecta since r-processing in the decompressing ejecta has been shown to produce abundance peaks around Calcium and Titanium (Jaikumar et al. 2007). We expect signatures of such a binary to be

- No Hydrogen, no Silicon but weak Helium lines (leftover Helium).
- Oxygen, Magnesium lines and perhaps Calcium lines

This is similar to the spectrum of some Type Ic supernovae that show weak He lines (Matheson et al. 2000). An important point in our model is that Calcium and Oxygen originate from different sources: Calcium from slow-moving QN ejecta that do not get completely pulverized upon impact and Oxygen from Helium-burning of the white dwarf.

5.2.4. *Regime 4: $T_{\text{WD}} < 8.6 \text{ keV}$, thermal ablation*

Nuclear burning is not possible in this system since Helium ignition cannot happen in this temperature regime, which corresponds to

$$a_{10} > a_{\text{O}} \quad (31)$$

If $a > a_{\text{th}}$, the extended emission will be weak, but if $a < a_{\text{th}}$, thermal ablation can still take place, according to the energetic arguments discussed in 5.1. We expect signatures of a QN in such a binary to be

- Strong Helium lines, no Hydrogen or Silicon lines
- α -elements such as Calcium and Titanium

This is similar to the spectrum of Type Ib supernovae, except that no Oxygen line should be seen. We note that the distinctions between the regimes may not be as clear cut as presented here, rather there should be a continuum of possibilities. A detailed calculation of the observed spectral features is beyond the scope of this work, but will be the subject of further studies.

5.3. *Duration and variability*

In our model, the extended emission immediately following the prompt emission (in the allowed regime) consists of emission of softer X-ray photons ($T_{\text{WD}} < T_{\text{CD,obs.}}$) with total energy output $\sim 10^{50} \text{ erg}$. Whether the WD is ablated thermally or ignited via nuclear reactions, the energy will be released within a dynamical time scale $\tau_d \sim (G\rho_{\text{WD}})^{-1/2} \sim 46.5 \text{ s}/M_{\text{WD},0.1}$.

The extended emission associated with short GRB tails are highly variable and in some cases on timescales less than $\sim 1 \text{ s}$ much less than typical duration ($\sim 100 \text{ s}$) of the tail (eg. Norris & Bonnell 2006). Currently, it is not clear how such variability can be accounted for in our model. One possible future avenue is to explore shock driven instabilities during the “crushing” of the WD or mechanisms that could drive radial oscillations of the WD between its RL radius, $R_{\text{WD,RL}}$, and R_{WD} .

6. LATE X-RAY ACTIVITY

6.1. *Nickel decay*

Systems experiencing a QN explosion while $a < a_{\text{Ni}}$ will process most of the WD into Nickel, which will decay $^{56}\text{Ni} \rightarrow ^{56}\text{Co}$ through energetic photons with energy $\sim 0.8 \text{ MeV}$ (Pinto et al. 2001). The resulting energy release is $\sim 1.7 \times 10^{48} \times M_{\text{WD},0.1} \text{ erg}$ in the X-ray. If released in 10^5 s ($\tau_{\text{Ni}} \sim 6 \text{ days}$) this corresponds to a luminosity of $\sim 10^{43} \text{ erg s}^{-1}$.

6.2. Accretion onto the Quark star

The fate of the WD ablated material depends on whether it can escape the system. Comparing the escape speed, $V_{\text{esc}} \sim 2 \times 10^3 \text{ km s}^{-1} M_{\text{QS},1.5}^{1/2}/a_{10}^{1/2}$, to $V_{\text{th.,eject.}}$ and $V_{\text{nuc.,eject.}}$ one can argue that, in general, part of the WD ablated material can be trapped. The trapped material could then be accreted onto the QS which could lead to X-ray activity beyond the EE discussed above. The corresponding duration can roughly be estimated as the free-fall time, $\tau_{\text{ff}} \sim 50 \text{ s} \times a_{10}^{3/2}/M_{\text{QS},1.5}^{1/2}$, where the QS mass is given in units of $1.5M_{\odot}$. If enough material is accreted in the process, the QS might turn into a black hole. The conversion of the QS to a black hole should lead to bursting events (X-ray spikes) occurring shortly after the EE. For systems with $a < a_{\text{Ni}}$ (with signatures of Nickel burning), the free-fall timescale and therefore the duration of the accretion activity from accretion is brief ($\lesssim 50 \text{ s}$). They should also show a late-time ($\sim 10^5 \text{ s}$) Nickel decay bump lasting for $\tau_{\text{Ni}} \sim 6 \text{ days}$. On the other hand, for $a > a_{\text{Ni}}$, the duration of the late X-ray activity could last as long as $\sim 10^3 \text{ seconds}$ and no ^{56}Co or ^{56}Fe lines should be present.

6.3. Quark-star spin-down

In the event that the QS does not turn into a black hole, it becomes a source of late X-ray activity. The QN compact remnant is a QS which consists of a vortex where the interior magnetic field is confined (Ouyed et al. 2004). These vortices are expelled as the star spins down releasing and dissipating its interior magnetic field (Ouyed et al. 2004; Niebergal et al. 2010a). For optimum conversion of spin-down energy to radiation, the resulting X-ray luminosity is

$$L_{\text{sd}} \sim 3.75 \times 10^{48} \text{ erg s}^{-1} \quad (32)$$

$$\left(\frac{B_0}{10^{15} \text{ G}} \right)^2 \left(\frac{2 \text{ ms}}{P_0} \right)^4 \left(1 + \frac{t}{\tau} \right)^{-5/3},$$

where $P_0 = P_{\text{NS,eq.}}$ (see eq.(3)) and B_0 are the birth spin period and magnetic field strength of the QS respectively; the QS magnetic field is given in units of 10^{15} G as found from studies of magnetic field generation in quark matter (e.g. Iwazaki 2005). The characteristic spin-down time (in seconds) is (Niebergal et al. 2006),

$$\tau_{\text{sd}} = 3.3 \times 10^3 \text{ s} \left(\frac{10^{15} \text{ G}}{B_0} \right)^2 \left(\frac{P_0}{2 \text{ ms}} \right)^2 \left(\frac{M_{\text{QS}}}{1.5 M_{\odot}} \right) \left(\frac{10 \text{ km}}{R_{\text{QS}}} \right)^4. \quad (33)$$

The curve from spin-down is flat for up to τ_{sd} before decaying at a rate $t^{-5/3}$ (different from the usual t^{-2} for the neutron star case because vortex expulsion in the QS case leads to faster magnetic field decay). The flat segment could end abruptly in the event the QS collapses to a BH because of spin-down and the subsequent increase of its core density (Staff et al. 2006). Finally, we note that the spin down energy will be released preferably along the equator and should naturally be observed together with the prompt emission.

7. CONCLUSIONS

In this paper we presented the idea of a Quark-Nova occurring in an LMXB (NS-WD binary) during or near the end of the first accretion phase. Our basic assumption of a detonative phase transition occurring in the massive neutron star in an LMXB leads to many interesting consequences. We found that several features of the short-hard GRBs can arise naturally in our model, with the binary separation playing an important role. Prompt emission occurs due to the interaction between the Quark-Nova ejecta and the circumbinary disk. Adopting a size and speed distribution for the chunks can explain the range of energetic photons observed (keV-TeV) as well as the duration of the prompt component. Most importantly, a statistical approach to the ejecta break-up and collision with the circumbinary disk could in principle lead to a light curve closely resembling the empirical Band function.

Extended emission in our model comes from ablation of the WD, either thermally or via nuclear ignition. Interestingly, the spectral features depend principally on the binary separation, and are expected to display many similarities to type I SNe. Thus, our model offers a plausible unification all the Type I Supernovae. Late X-ray activity is explained in terms of Nickel decay and accretion of gravitationally trapped material onto the Quark star. It may or may not become a black hole, and X-ray activity can result in either case; in the former it will consist of X-ray spikes while in the latter, it will be the quiescent spin-down luminosity of the QS. Afterglows are explained in terms of synchrotron radiation from the rapidly expanding shocked circumbinary disk material. In all cases, the energetics provide the correct order of magnitude.

The rarity of short GRBs calls for rare situations/events. Our model suggests Quark-Novae in LMXBs born with heavy Neutron Stars are the likely engines of the burst. The universality of our model can be confirmed if it turns out that indeed heavy neutron stars ($> 1.6M_{\odot}$) in LMXBs are associated with or favor the formation of circumbinary disks. The characteristics of the disk (e.g. size, density etc ...) are expected to vary slightly from one system to another which could explain differences in burst duration, apparent energy release and spectra.

If our model is a correct representation for short-GRBs engines, most of these engines would reside in globular clusters (GCs) where many LMXBs are seemingly found (Bogdanov et al. 2006; Camilo & Rasio 2005). It also implies that short GRBs should be associated with early-type galaxies (no spiral arms) known to form their LMXBs in GCs. There is some evidence that short GRBs reside in the outskirts of early-type galaxies (Fox&Roming 2007) where many GCs are located. Finally, the WD ablation in our model provides a potential unifying framework for the central engines of type I Supernovae. In particular, systems observed at high latitudes (i.e. $> H/R$) when the QN goes off, could find some interesting applications in the context of unusual type Ia SNe (e.g. SN2005E; Perets et al. (2010)) and/or subluminal type Ia SNe in general (González-Gaitán et al. (2010)).

The research of R. O. is supported by an operating grant from the National Science and Engineering Research Council of Canada (NSERC). P. J. acknowledges start-up funds from California State University Long Beach. This work has been supported, in part, by grants AST-0708551, PHY-0653369, and PHY-0326311

from the U.S. National Science Foundation and, in part, by grant NNX07AG84G from NASA's ATP program. J. S. and R. O. are grateful for the hospitality at California State University Long Beach and San Diego State University during this work.

REFERENCES

- Akmal, A., Pandharipande, V. R., & Ravenhall, D. G. 1998, *Phys. Rev. C*, 58, 1804
- Åström, J. A., et al. 2004, *Phys. Rev. E*, 70, 026104
- Åström, J. A. 2006, *Advances in Physics*, 55: 3, 247
- Band, D., et al. 1993, *ApJ*, 413, 281
- Barthelmy, S. D., et al. 2005, *Nature*, 438, 994
- Baym, G., Pethick, C., & Sutherland, P. 1971, *ApJ*, 170, 299
- Belle, K. E., Sanghi, N., Howell, S. B., Holberg, J. B., & Williams, P. T. 2004, *AJ*, 128, 448
- Berger, E. 2007, *ApJ*, 670, 1254
- Bhattacharya, D. & van den Heuvel, E. P. J. 1991, *Phys. Rep.*, 203, 1
- Blattnig, S., Swaminathan, S., Kruger, A. T., Ngon, M. & Norbury, J. 2000, *Phys. Rev. D* 62, 094030
- Bloom, J. S. & Prochaska, J. X. 2006, *Am. Inst. Phys. Conf. Ser.* 836, 473.
- Bodmer, A. R. 1971, *Phys. Rev. D*, 4, 1601
- Bogdanov, S., Grindlay, J. E., Heinke, C. O., Camilo, F., Freire, P. C. C., & Becker, W. 2006, *ApJ*, 646, 1104
- Bowler, M. G. 2010 [arXiv:1012.4689]
- Brown, W. K. & Wohletz 1995, K. H., *Journal of Applied Physics*, Vol. 78, No. 4, 2758.
- Buehler, M. J. & Gao, H. 2006, *Nature* 439, 307
- Camilo, F., & Rasio, F. A. 2005, *Binary Radio Pulsars*, 328, 147
- Cho, H. T., Ng, K.-W. & Spiliotopoulos, A. D. 1994, *Phys. Lett. B*, 326, 111
- Cordes, J. M. & Shannon, R. M. 2008, *ApJ*, 682, 1152
- Covino, S., et al. 2005, *GRB Coordinates Network*, 3665, 1
- Dai, Z. G., Wang, X. Y., Wu, X. F. & Zhang, B. 2006, *Science*, 311, 1127
- Datta, B., Thampan, A. V., & Bhattacharya, D. 1995, *Journal of Astrophysics and Astronomy*, 16, 375
- Drago, A., Lavagno, A., & Parenti, I. 2007, *ApJ*, 659, 1519
- Dubus, G. et al. 2002, *ApJ* 569, 395
- Dubus, G., Campbell, R., Kern, B., Taam, R. E., & Spruit, H. C. 2004, *MNRAS*, 349, 869
- Fox, D. B. & Roming, P. W. A. *Phil. Trans. R. Soc. A* 2007 365, 1293
- Frank, J., King, A., & Raine, D. J. 2002, *Accretion Power in Astrophysics*, by Juhan Frank and Andrew King and Derek Raine, pp. 398. ISBN 0521620538. Cambridge, UK: Cambridge University Press, February 2002.
- Gentile, N. A., Aufderheide, M. B., Mathews, G. J., Swesty, F. D., & Fuller, G. M. 1993, *ApJ*, 414, 701
- Ghosh, P. & Lamb, F. K. 1992, in *X-ray Binaries and Recycled Pulsars*, eds. E. P. J. van den Heuvel & S. A. Rappaport (Kluwer: Dordrecht), 487
- González-Gaitán, S. et al. 2010 [arXiv/1011.4531]
- Handbook of Chemistry and Physics 2005, B-1 (CRC Press)
- Heinz, S. & Begelman, M. 1999, *ApJ*, 527, L35
- Horowitz, C. J., & Kadau, K. 2009, *Physical Review Letters*, 102, 191102
- Horvath, J. E. & Benvenuto, O., G. 1988, *Phys. Lett. B*, 213, 516
- Horvath, J. E. 2010, arXiv:1005.4302 [astro-ph.HE]
- Itoh, N. 1970, *Prog. Theor. Phys.* 44, 291
- Iwamoto, N. 1989, *Phys. Rev. A*, 39, 4076
- Iwazaki, A. 2005, *PhRvD*, 72, 114003
- Jaikumar, P., Meyer, B. S., Otsuki, K., & Ouyed, R. 2007, *A&A*, 471, 227
- Keränen, P., Ouyed, R., & Jaikumar, P. 2005, *ApJ*, 618, 485
- King, A., Olsson, E., & Davies, M. B. 2007, *MNRAS*, 374, 34
- Klein, R. I., McKee, C. F., & Colella, P. 1994, *ApJ*, 420, 213
- Landau, L. D. & Lifschitz, E. M. 1959, *Fluid Mechanics*, Oxford: Pergamon Press
- Lazzati et al. 2010, *ApJ*, 717, 239
- Lin, J., Rappaport, S., Podsiadlowski, P., Nelson, L., Paxton, B., & Todorov, P. 2010, arXiv:1012.1877
- Linna, R.P., Åström, J. A., & Timonen, J. 2004, *Comp. Phys. Comm.* 158, 26
- Matheson, T., Fillipenko, A., Chornock, R., Leonard, D. & Li, W. 2000, *ApJ*, 119, 2303
- Mazets, E. P., et al. 2004, *ASPC*, 312, 102
- Metzger et al. 2008, *ApJ*, 385, 1455
- Muno, M. P. & Mauerhan, J. 2006, *ApJ*, 648, L138
- Nakar, E. 2007, *Phys. Rep.*, 442, 166
- Niebergal, B., Ouyed, R., & Leahy, D. 2006, *ApJ*, 646, 17
- Niebergal, B., Ouyed, R., Negreiros, R., & Weber, F. 2010a, *Phys. Rev. D*, 81, 3005
- Niebergal, B., Ouyed, R., & Jaikumar, P. 2010b, *Phys. Rev. C* 82, 062801 [arXiv:1008.4806 [nucl-th]]
- Norris, J. P. & Bonnell, J. T. 2006, *ApJ*, 643, 266
- Norris, J. P., & Gehrels, N. 2008, *American Institute of Physics Conference Series*, 1000, 280
- Olinto, A. V. 1987, *Phys. Lett. B.*, 192, 710
- Ouyed, R., Dey, J., & Dey, M. 2002, *A&A*, 390, L39
- Ouyed, R., Elgarøy, Ø., Dahle, H., & Keränen, P. 2004, *A&A*, 420, 1025
- Ouyed, R., Rapp, R., & Vogt, C., 2005, *ApJ*, 632, 1001
- Ouyed, R., & Leahy, D. 2009, *ApJ*, 696, 562
- Ouyed, R., Leahy, D., Staff, J., & Niebergal, B. 2009, *Adv. Astr.*, 2009, 2
- Ouyed, R., Kostka, M., Koning, N., Leahy, D., & Steffen, W. 2010, arXiv:1010.5530
- Özel, F. & Psaltis, D. 2009, *Phys. Rev. D*, 80, 103003
- Paczynski, B. 1971, *ARA&A*, 9, 183
- Perets, H. B., et al. 2010, *Nature*, 465, 322
- Perna, R., Armitage, P. J., & Zhang, B. 2006, *ApJ*, 636, 29
- Pinto, P. A., Eastman, R. G., & Rogers, T. 2001, *ApJ*, 551, 231
- Piran, T. 2001, 20th Texas Symposium on relativistic astrophysics, 586, 575
- Proga, D. & Zhang, B. 2006, *MNRAS*, 370, 61
- Rhoads, J. E. 1997, *ApJ*, 487, L1
- Rosswog, S. 2006, *Superdense QCD Matter and Compact Stars*. eds. D. Blaschke and D. Sedrakian. *Proceedings of the NATO Advanced Research Workshop*, p.309 (Springer, Dordrecht, The Netherlands)
- Russo, G. 1988, *ApJ*, 334, 707
- Savonije, G. J. 1983, *Nature*, 304, 422
- Sharon, E., Gross, S. P. & Fineberg, J. 1995, *Phys. Rev. Lett.* 74, 5096
- Sharon, E. & Fineberg, J. 1996, *Phys. Rev. B* 54, 7128, 1996
- Staff, J., Ouyed, R., & Jaikumar, P., 2006, *ApJ*, 645, L145
- Taam, R. E. & Spruit, H. C. 2001, *ApJ*, 561, 329
- Taam, R. E., Sandquist, E. L., & Dubus, G. 2003, *ApJ*, 592, 1124
- Umeda, H. 2000, *ApJ*, 528, L89
- Verbunt, F. 1993, *ARA&A*, 31, 93
- Villasenor, J. S., et al., 2005, *Nature*, 437, 855
- Vogt, C., Rapp, R., & Ouyed, R. 2004, *Nuc. Phys. A*, 735, 543
- Wang, Z., Chakrabarty, D., & Kaplan, D. L. 2006, *Nature*, 440, 772
- Watts, A. L., & Strohmayer, T. E. 2007, *Advances in Space Research*, 40, 1446
- Weibull, W. 1939, *The Royal Swedish Institute of Engineering Research*, Proc. no. 151
- Witten, E. 1984, *Phys. Rev. D*, 30, 272
- Yoffe, E. H. 1951, *Phil. Mag.* 42, 739
- Zhang et al. 2007, *ApJ*, 655, 989